NASA TECHNICAL NOTE

NASA TN D-2755

NASA TN D-2755

SHADOWGRAPH STUDY OF THE UPPER STAGE FLOW FIELDS OF SOME SATURN V STUDY CONFIGURATIONS IN THE TRANSONIC MACH NUMBER RANGE

by C. Dale Andrews and David R. Carlson

George C. Marshall Space Flight Center
Huntsville, Ala.

NATIONAL AERONAUTICS AND SPACE ADMINISTRATION • WASHINGTON, D. C. • APRIL 1965

NASA TN D-2755

SHADOWGRAPH STUDY OF THE UPPER STAGE FLOW FIELDS OF SOME SATURN V STUDY CONFIGURATIONS IN THE TRANSONIC MACH NUMBER RANGE

By C. Dale Andrews and David R. Carlson

George C. Marshall Space Flight Center
Huntsville, Ala.

NATIONAL AERONAUTICS AND SPACE ADMINISTRATION

For sale by the Clearinghouse for Federal Scientific and Technical Information
Springfield, Virginia 22151 – Price $2.00

TABLE OF CONTENTS

LIST OF ILLUSTRATIONS

DEFINITION OF SYMBOLS

Symbol	Definition
α	Angle of attack, degrees
δ	Boundary layer thickness
M	Mach number
ρ	Density
Re	Reynolds number based on reference diameter

SHADOWGRAPH STUDY OF THE UPPER STAGE FLOW FIELDS OF SOME SATURN V STUDY CONFIGURATIONS IN THE TRANSONIC MACH NUMBER RANGE

SUMMARY

This report presents graphical engineering interpretations of selected shadowgraphs. The photographs were obtained during transonic wind tunnel tests of two preliminary Saturn V study configurations, mostly by MSFC's 14-inch trisonic tunnel. The engineering interpretations are intended to be qualitative aids in the evaluation of space vehicle aerodynamic data in the critical transonic Mach number range. They should be particularly valuable in (a) the determination of the degree of applicability of analytical tools in view of the flow fields and their interactions; (b) the support and explanation of test results, particularly where anomalies are observed; and (c) the prediction of areas of extremely fluctuating pressures.

The interpretations show the effects of Mach number, angle of attack, and launch escape system spikes on the flow fields about the unconventional Saturn upper stage shapes. Background information is given on the pictorial fidelity, problems of interpretation of shadowgraphs, separable Reynolds and Mach number effects, spike effects, and shock-boundary layer interactions. The applicability of test results to full scale flow fields is argued. A detailed discussion dissects the sample interpretations and lists characteristics of typical flow fields.

The most significant conclusions are as follows:

1. The tests simulate flight vehicle flow fields very well, despite some Reynolds number disparities.

2. Conventional exact attached-flow theoretical concepts are generally inapplicable.

3. Large areas of separated flow, sensitive to angle of attack, cover the vehicle.

4. Local supersonic flows are initially felt on the body at Mach numbers near 0.8.

5. Strong shock-boundary layer interactions occur on or near frustums, with the shocks impinging on unsteady mixing regions. This indicates presence of fluctuating pressures.

SECTION I. INTRODUCTION

Early launch vehicles were simple configurations, usually consisting of spherically-blunted cones joined to cylinders. Flow field disturbances radiated by such shapes were usually confined to the nose region, and their paucity allowed analysts to predict aerodynamic characteristics very well from theory. The advent of unconventional Saturn-type configurations has signalled the exit of good theoretical predictions based on the inviscid equations in the transonic and low supersonic regimes. Only in the hypersonic range does inviscid theory again come into its own. The main reasons for the poor theoretical correlations are the large areas of separated flow on the vehicle and lack of a suitable theory for prediction and analysis of such separation.

The typical Saturn shape is a blunt cone-cylinder followed by a succession of conical frustums of varying angle and cylinders of varying length. Wind tunnel tests on such shapes began about four years ago. It was immediately realized that pictorial records of the flow fields were an indispensable aid to the analysis of Saturn's aerodynamic characteristics. The most critical area is the transonic-low supersonic range, where theory fails and where dynamic pressures are greatest. As testing progressed, investigators found that good optical coverage was also required at high Mach numbers, where shock-boundary layer interactions sometimes caused large changes in characteristics.

While shadowgraphs provide the least amount of quantitative information compared with interferometric and Schlieren systems, they are ideal for visualizing the disturbances in a flow field. An advanced spark shadowgraph system was developed which yielded the required brilliance and high degree of resolution. This system was the result of a fine-tooth-comb improvement of the controlling factors -- size, intensity and duration of the spark; its geometric mating to the test condition; and the right choice and processing of photosensitive materials. Reference 1 describes the mechanical detail of the equipment and some aspects of spark photography in general.

This paper presents engineering interpretations of shadowgraphs (Figs. 2 and 3) taken during tests of typical Saturn shapes, most of which were conducted at the MSFC 14-inch Trisonic Tunnel [2]. Included interpretations show the effects of Mach number, angle of attack, and launch escape system "spikes" on upper stage flow fields. The effect of Reynolds number variation has not been included because of the limited range available in MSFC's facility. Actual shadowgraphs (two of which appear as Figure 4) are the basis of these interpretations.

The paper is motivated by three factors. First, project engineers have accumulated volumes of flow visualization records without being able to easily disseminate them among other engineers. Second, mass reproduction of these records is impossible without severe loss of detail (the cost is prohibitive). Third, many of the pictures need interpretative comment to cull the optical distortions, window striations, and shock reflections.

The illustrations are more than artist's conceptions. Many references were consulted during their preparation. Records from different sources were compared, and parametrically similar situations were interpolated to construct the most realistic and proportionally correct illustrations for the cases chosen. For this reason, the illustrations are described as engineering interpretations. Interpretation is not always straightforward. Personal opinion unavoidably enters the problem and has done so in this report. The authors welcome any comments.

The authors wish to acknowledge the contributions of the staff of the Aerodynamic Design Branch, and particularly those of Mr. G. Pertree, who performed the art work for the engineering interpretations.

SECTION II. MODEL AND FACILITY DESCRIPTION

A. MODELS

The subject models were two 0.0033-scale preliminary Saturn V configurations, the exact geometries of which are shown in Figure 1. Neither is fully representative of the latest designs; however, dimensional obsolescence is immaterial to the purposes of this paper. The lower model of Figure 1 is more nearly representative of current designs.

These particular models were chosen for two reasons. First, many shadowgraphs were available, especially for Model B, the more current shape. Second, Model A is a much more slender body than is Model B. Its leading frustum is of smaller cone angle and is less prone to separation and to generation of strong shocks in the low supersonic range. Therefore, although both models have two cylinders and two frustums, the overall flow fields are quite different. These interpretations then provide a qualitative assessment of the effects of slenderizing the upstream portions of a model.

B. WIND TUNNEL

The tests were conducted in MSFC's 14-inch trisonic tunnel. Two test sections provide a Mach number range between 0.4 and 5.0. A unique design feature of the tunnel is the capability of quick interchange of these test sections.

Mach numbers between 0.4 and 2.0 are achieved with a "transonic" test section, which uses fixed nozzle blocks, movable perforated walls, auxiliary suction, and flaps. The high range, Mach 2.7 through 5.0, is achieved with a fixed-contour variable Mach number supersonic nozzle. The blowdown tunnel exhausts to either atmospheric pressure or vacuum. Automatically controlled high-pressure storage batteries supply dry air at stagnation pressures of up to seven atmospheres. The air passing through the stilling chamber is heated to a maximum of 200° F by a capacity-type heat exchanger.

It then passes through flow straighteners and three damping screens before entering the contraction section. Reference 2 further describes the facility and presents flow calibrations.

C. SHADOWGRAPH SYSTEMS

Spark shadowgraphs are taken by a Fairchild A-7 aerial camera magazine, loaded with 75-foot reels of film, through windows in the transonic test section. The spark source is located on the opposite side of the tunnel in an opaque conical cover. The film is placed as close to the window as possible, and the light source is translated within its conical cover to change magnification.

The camera has been modified so that manual signal by the tunnel operator exposes and advances the film. Automatic equipment processes the exposed film, and negatives can be viewed approximately ten minutes after exposure. Reference 1 provides further details of the process.

SECTION III. SHADOWGRAPH APPLICATION AND VALIDITY

All flow-visualization techniques rely on density variations for their results. Interferometers measure density levels compared with some reference state; fringe shifts are counted to obtain variations in density. Schlieren systems show gradients in density (first x-derivative), and shadowgraphs show the gradient of density gradient (second x-derivative).

Figure 5 illustrates relative intensities for the flow across a normal shock wave. The shock will show up as a wider disturbance in the shadowgraph, and the characteristic white line on the downstream side of the shock is a consequence of the negative second derivative. Relative shock strengths are easily seen on a shadowgraph, but difficulties inherent in the performance of a double integration of photographic intensity automatically preclude the determination of actual density levels.

Boundary layers and separated regions show up nicely in shadowgraphs if the flow field density is not too low. Here we must be careful. Density changes across shocks and expansions are governed by ratios which are functions of Mach number and flow direction. Density gradients (changes with distance) depend on these ratios and on upstream density levels. Hence, disturbances in a low-density flow will not be as visible on a shadowgraph as those in a high-density flow. Two effects applied to boundary layers become apparent. First, large variations of density occur only in the lower viscous strata, especially if the layer is turbulent. Thus the thickness of a boundary layer seen in a shadowgraph is less than its actual thickness. Second, the boundary layer downstream of a corner expansion often appears to be thinner than it was upstream.

This effect is entirely due to reduction in density level and to transient changes in the transverse thermodynamic profiles.

An axially symmetric flow field is not as easy to analyze as a two-dimensional field. Boundary layers are thinner, shocks are weaker, and the parallel light rays penetrating a three-dimensional field pick up extraneous disturbances which must be mentally weeded out. Engineering interpretations are especially valuable in the exclusion of the extraneous images.

Before assessing the validity of the shadowgraphs (as they apply to the full scale vehicle), we briefly review some basic characteristics of interacting flow fields. Compression and expansion waves, and their strengths and locations, are strongly dependent on Mach number but only weakly so on Reynolds number. On the other hand, boundary layer development and, in the absence of shocks, separated regions are strong functions of Reynolds number. When viscous layers and waves occur at the same place, interactions result which are sensitive to Mach-Reynolds number combinations. Such interactions occur at nearly every geometric discontinuity at transonic and supersonic speeds.

The boundary layer on a smooth blunt body follows a negative (favorable) pressure gradient around the body. A simple sharp spike on the nose will drastically alter the flow field. In this case, the boundary layer developing on the spike fights an increasing pressure as it approaches the stagnation point. At some point, the location of which depends on whether the layer is laminar or turbulent, it separates from the spike and creates a large recirculating dead-air region on the nose. This effect is characteristic of the configurations with the launch escape system (LES).

Because the lower strata of a boundary layer are subsonic, no waves reach the body. Thus the adverse surface pressure gradient associated with a shock must be more gradual than it is in the free stream. The distance over which the pressure rises is called the width of diffusion [3] and is about 10δ for a turbulent layer and 100δ for a laminar layer. Local separation is highly probable when a shock and boundary layer interact, but its extent is much larger in the laminar case. Whether separation occurs or not, the boundary layer thickens ahead of the shock.

Attached laminar layers can only support small pressure rises. After separation, however, a laminar free-mixing layer can overcome large pressure rises. Hence, a layer which is laminar at separation may still be laminar at reattachment. If the shock is strong (high Mach number) but the Reynolds number is low, a laminar layer will separate ahead of the shock and may or may not undergo transition at the same time. At high Reynolds numbers, transition will occur ahead of the shock whether separation occurs or not.

In his studies of supersonic diffusers, Busemann discovered that, at all Mach numbers, separation did not depend on angle of convergence or divergence; but it could

always be associated with an adverse pressure gradient. In general, turbulent boundary layers will not separate unless there is at least an 80 percent rise in pressure over the narrow width of diffusion.

With the above discussion in mind, we postulate that the illustrations are representative of the flow fields about the full scale vehicle at corresponding Mach numbers and low angles of attack, even though test Reynolds numbers were off by a factor of 100 ($\doteq 10^6$ versus $\doteq 100 \times 10^6$ full scale). Ignoring minor artistic liberties, we have full confidence in the correctness of the important basic features of the flow fields. In other words, we believe that the gross effect of Reynolds number differences is small under these conditions. This should not be construed as an invitation to scale boundary layer thicknesses (see the earlier discussion on boundary layers in shadowgraphs), but it is believed that shock shapes and other flow field quantities are similar to those on the flight vehicle.

This declaration of confidence is supported by theoretical and experimental evidence. The test Reynolds numbers are high enough that, whether the LES spike is on or off, the boundary layer is certainly turbulent before its first interaction with a shock wave. From this point on, a higher Reynolds number has very little effect on the occurrence or extent of separation.

For Saturn vehicles, the simulation of full scale Reynolds number is impossible in any existing transonic test facility. Full scale simulation is possible, however, for Mach numbers of the order of three and above. Such tests have been conducted [4]. The inability to duplicate Reynolds number is not unique with Saturn; only the degree of disparity is new.

SECTION IV. CHARACTERISTICS OF TYPICAL SATURN FLOW FIELDS

The engineering interpretations included in this report show the effects of variations in Mach number, geometry and attitude on the gross flow-field features of Saturn shapes. As we stated above, Reynolds number effects are not included because of limited test range, but their inclusion is believed unnecessary anyway. Comparison of Figures 3c, 3d, and 4 shows that the shapes and locations of the significant flow field features are unaltered in the interpretation, while the confusing waves are deleted.

The subject models appear in Figure 1. All linear dimensions are given in calibers. Lengths and angles (particularly those of the leading frustums) differ from each other and from current designs, but this fact has no bearing on the aims of this report.

Figure 2 shows the flow field about Model A as the Mach number increases from 0.7 to 1.2. One fact stands out: theoretical attached-flow concepts are totally inadequate for the analysis of such shapes in the transonic range.

At M = 0.7, the boundary layer separates right at the cone-cylinder junction, drowns the first frustum in "dead air," and reattaches on the long cylinder. No further separation occurs at the second frustum-cylinder junction, probably because the local, equivalent-flat-plate Reynolds number excludes that possibility. Note that the layer thickens at the head of the second frustum and then thins out as the aft juncture is approached and passed. This thinning effect is probably caused by a combination of decreasing density on the frustum and alteration of the thermodynamic profiles by centrifugal forces at the aft juncture. Again, we caution that boundary layer thicknesses are not to be scaled.

At M = 0.8, the turbulent separated region extends farther downstream before reattaching. In this case, the reattached boundary layer remains thick over the whole body. The aft-frustum expansion to locally supersonic flow causes an apparent thinning; this trend is reversed by the system of weak normal shocks on the aft cylinder.

The separated flow region at M = 0.9 is less extensive than it was at M = 0.8, and a weak normal shock system perturbs its boundaries. The boundary layer is thick up to the frustum, where compressive forces make it thinner. Again, the corner expansion produces locally supersonic flow and an apparently thinner boundary layer. A semi-normal recompression shock appears on the aft cylinder.

Sonic velocities (M = 1.0) herald more complicated flow fields. Expansion waves emanate from the cone-cylinder junction. The mixing layer seems to have thinned a bit, but the former normal shock system has changed to a conical recompression shock attached to the forward frustum. Overexpansion at the shoulder causes slightly supersonic speeds. The flow is then sent subsonic by a weak conical recompression and a normal shock. The boundary layer remains thick up the compressing second frustum surface. At the aft juncture, the flow overexpands and recompresses in a short distance. The downstream Mach number is just slightly supersonic, and a normal shock takes care of that.

The forward separation region has definitely decreased its extent at M = 1.1. A typical bow shock is now present, and the cone-cylinder expansion is also there. The effective angle of the first frustum, decreased by the separated flow, generates an attached conical shock (a weak overexpansion and recompression force reattachment). The next shock, obviously a detached shock induced by the second frustum, thickens the boundary layer further. The final shoulder expansion and weak recompression apparently thin out the boundary layer, but this is a matter of speculation.

The highest Mach number tested, 1.2, is characterized by a conspicuous absence of separated flow at the forward end and a thin boundary layer on the body. The disappearance of the forward separated region at higher Mach numbers agrees with the data of Kuehn [5]. The forward frustum shock is still conical, but it would detach with a small increase in frustum angle. The second frustum shock induces local turbulent separation. It is difficult to ascertain whether this shock is truly a detached shock

or whether it is attached to the equivalent frustum generated by the free mixing layer. The shadowgraph seems to indicate the latter. The strength of the shock, in terms of pressure rise, is definitely greater than its counterpart at M = 1.1; otherwise, no local separation would occur. The unsteadiness of this mixing region is evident from the feathering of its shock wave near the body. The mixing layer reattaches just before going through the final expansion, and the subsequent boundary layer seems to be thin.

Figure 3 shows the effects of variation in Mach number, addition of the LES, and change in attitude of Configuration B. The cylindrical portions of this model are more nearly equal in length, and the forward frustum angle is greater than in the case of Configuration A. All in all, Configuration B is more representative of current configurations.

Figure 3a illustrates the large effect of the LES at M = 0.9. With the tower off, the layer separates at the cone-cylinder shoulder and does not reattach again until it impinges on the second frustum. The fluid then expands through sonic speed at the shoulder and culminates in a normal shock. Addition of the LES provokes a completely different flow field. The only separated region lies between the LES rocket and the command module. The attached boundary layer then traverses three local supersonic expansions and recompresses each time via weak normal waves. It seems to thicken as each frustum is approached and to thin out in each supersonic region. The final cylinder expansion and recompression is weaker than in the tower-off case.

Figures 3b and 3c show the effects of tower addition and subsequent pitch-up at sonic velocity. The tower-off configuration again shows a strong separation at the nose cone shoulder and reattachment back on the aft cylinder. The first frustum generates a detached shock, its position being somewhat sensitive to the mixing layer contour. After an expansion, a dished shock wave on the second cylinder, thought to be a product of both shoulder recompression and influence of the second frustum, decelerates the flow further. The extent of supersonic flow on the aft cylinder is considerably larger than it was at M = 0.9. The normal shock is still on the aft cylinder. The flow velocity would not return to sonic value until far downstream in the wake. The tower-on flow field resembles its counterpart at M = 0.9, except that (1) the boundary layer is thinner, (2) the shocks and expansions are stronger, (3) the shocks are further aft, and (4) the regions of supersonic flow are larger (much larger as we follow the flow downstream).

Only one significant change occurs in the flow as the model is pitched up, but it is very important from the standpoint of the forces and moments. The mixing layer induced by the LES flare misses the nose cone on the leeward meridian, inducing separated flow and causing a significant change in pressure differential. Further pitch-up merely increases the area of the vehicle covered by the separation. The leeward sides of the shocks weaken and move slightly forward in the body coordinates, while the windward sides strengthen and move slightly aft. The results are large negative pressure coefficients. The boundary layer on the windward side is thinner because of the higher compression.

Figures 3d and 3e follow the format of Figures 3b and 3c for Mach 1.2. As Kuehn [5] predicted, the separated volume decreases on the tower-off shape as Mach number increases. The frustum shocks induce turbulent separation in the corners, and the tendency toward reattachment is rapid. Though the shocks stand away from the frustums, they resemble attached conical shocks. It is believed that they are such, and that the corresponding body angles and apex locations are effective values determined by the displacement thickness distribution of the separating boundary layer. The bow shock is, of course, detached.

At this Mach number, addition of the LES increases the amount of separated flow. The surface Mach number is not high enough to allow the upstream frustum shock to attach to the effective frustum defined by the shock-induced separation. However, the downstream frustum shock does seem to be attached to the effective frustum. Small angle of attack increases the separation on the leeward side and causes an attached boundary layer on the windward side. In addition, the windward and leeward portions of the frustum shocks definitely assume attached and detached forms, respectively. The leeward sides of the shocks feather into weak waves near the body.

Figure 3f considers only angle of attack effects on the tower-on shape at M = 1.43. Now the surface Mach number is high enough that the separated boundary layers observed at M = 1.2, $\alpha = 0°$ are forced back on the body. The frustum shocks are definitely attached, and the boundary layer is thinner. The shock attached to the LES flare is quickly weakened by expansion waves from the end of the flare. A new shock appears where the tower-induced mixing layer impinges on the nose cone. It unravels into the unsteady tower mixing layer, but seems to be of an attached form. (The curvature observed does not begin until the point where expansion waves from the cone-cylinder junction would hit the shock.) A 3-degree angle of attack induces separation on the leeward meridian. The leeward sides of the shocks are all weaker, and the windward sides are stronger. The windward boundary layer is thinner, and the windward portion of the nose cone shock still seems to be attached. At $\alpha = 6°$, the leeward separation is very extensive and seems about to cover the whole model length. The nose cone shock emanates from approximately the same position as at $\alpha = 3°$, but now is curved closer to the body. This is probably caused by waves from the impingement region.

Figure 3g shows the same model at M = 1.93. The flow fields are similar to those of M = 1.43. Both the LES-flare shock and the nose cone shock move slightly aft, and all shocks are now attached. Any shock curvature observed is the result of impinging compression waves or rarefactions. The boundary layers are thinner, and the free mixing layer on the leeward side at angle of attack has a well-behaved contour. At $\alpha = 6°$, nearly the whole leeward meridian is separated. Figure 4 shows two of the higher quality shadowgraphs used in the construction of the engineering interpretations. Both are of Configuration B. The upper photo was used to draw Figure 3d, and the lower photo resulted in Figure 3c.

SECTION V. CONCLUSIONS

Engineering interpretations of shadowgraphs, such as those presented herein, are valuable aids to the analysis of the aerodynamic characteristics of unconventional configurations. They can be easily and cheaply reproduced; they can be annotated for clarity, and meaningless, but confusing, waves, reflections and striae are removed.

The test Reynolds numbers were high enough that the pictured flow field and the full scale flow field will correspond directly for low angles of attack. For gross effects, Reynolds number independence is declared in this Mach number range.

The usual exact, attached-flow theoretical concepts cannot be used to predict transonic and low-supersonic characteristics on these shapes.

Large areas of the vehicle are immersed in regions of separated flow. The peripheral distribution of these regions is highly sensitive to angle of attack.

In the transonic range, subsonic and supersonic velocities alternate on the vehicle. Local supersonic flow and associated compression waves first occur near $M = 0.8$.

Strong shock-wave boundary-layer interactions occur on or near the frustums, with the shocks often riding on or near the roots of the separations. The mixing layers are unsteady, and the Chapman concept of smooth recirculating flow in separated regions obviously does not apply. These phenomena are indicators of fluctuating pressures.

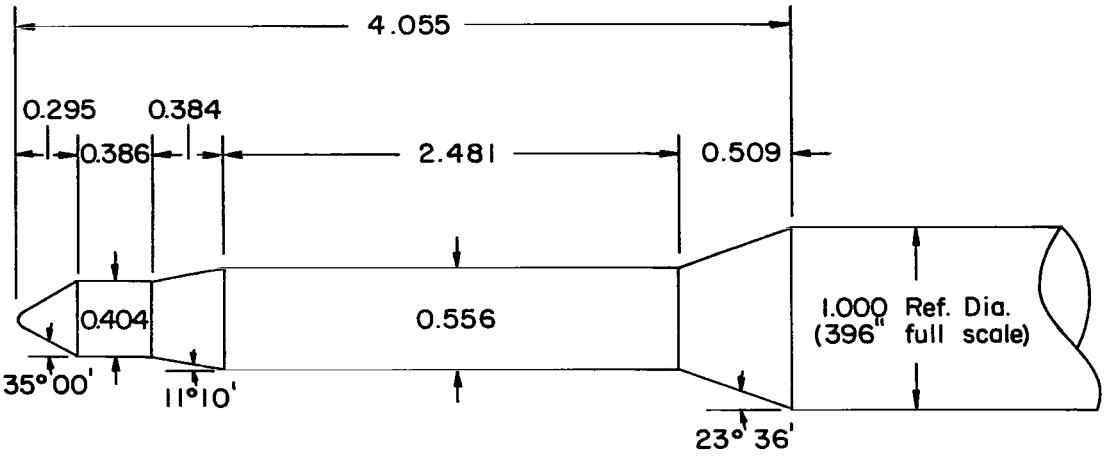

Configuration "A"

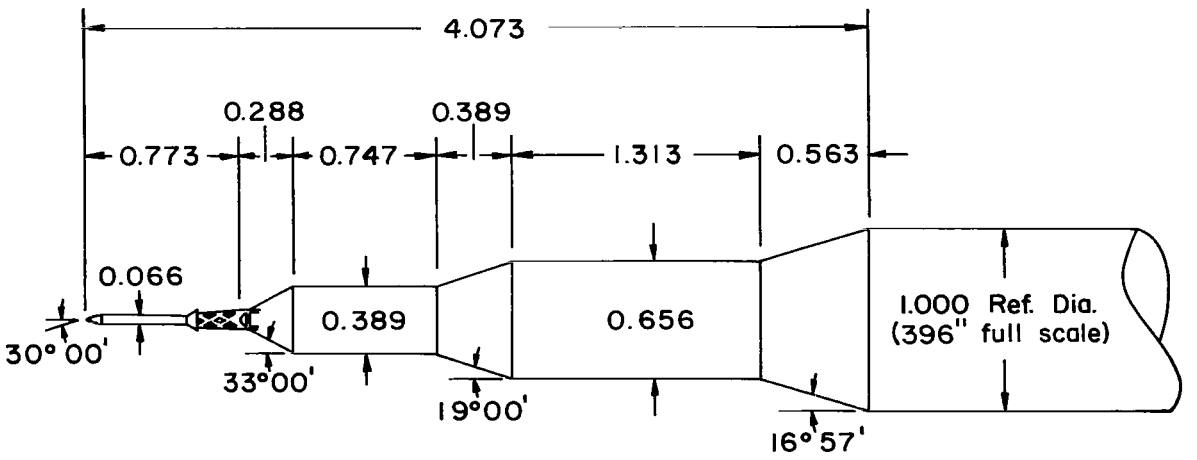

Configuration "B"

FIGURE 1. UPPERSTAGE GEOMETRY OF SHADOWGRAPH STUDY CONFIGURATIONS
(All Linear Dimensions in Calibers)

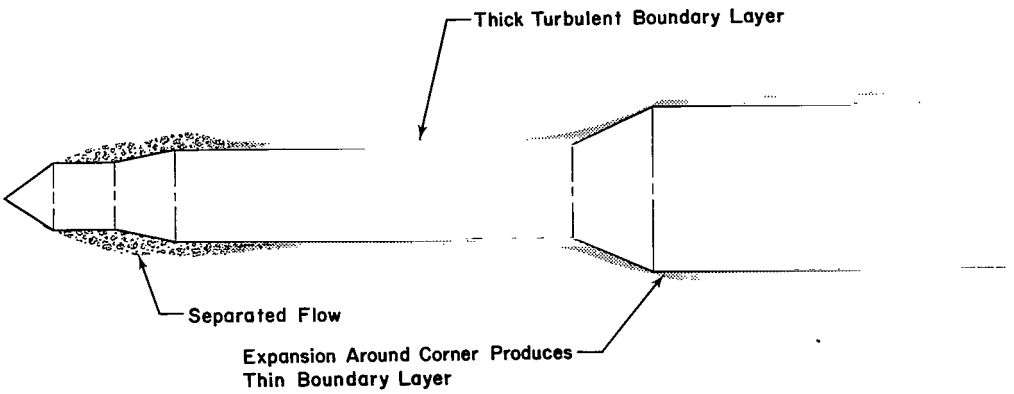

Free Stream Conditions
M=0.70 Re=0.60 x 10⁶
α=0°

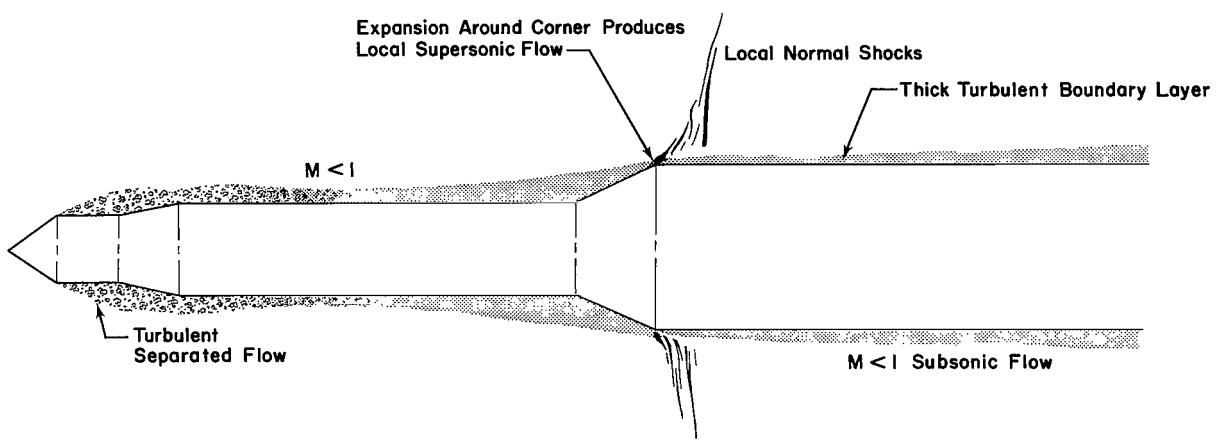

Free Stream Conditions
M=0.80 Re=0.64x10⁶
α=0°

FIGURE 2a. EFFECT OF MACH NUMBER ON UPPER STAGE FLOW FIELDS, CONFIGURATION "A," $\alpha = 0°$

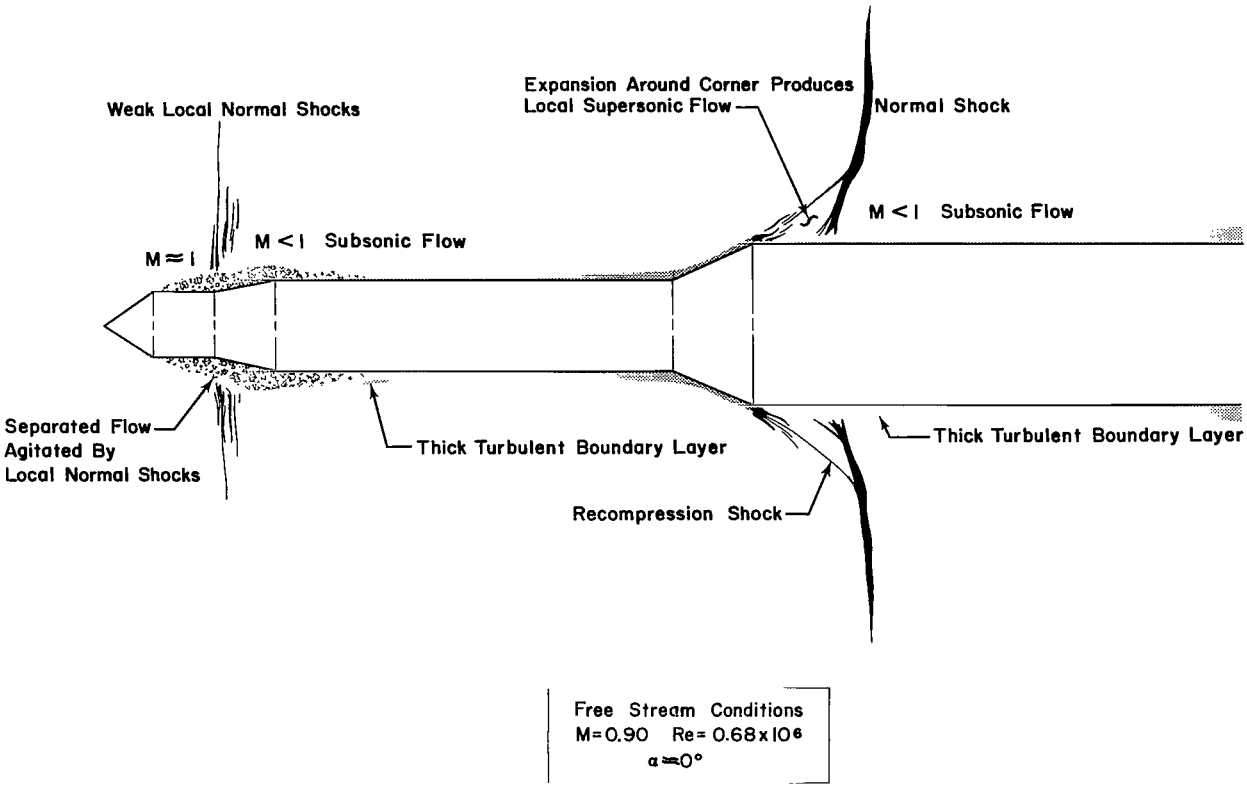

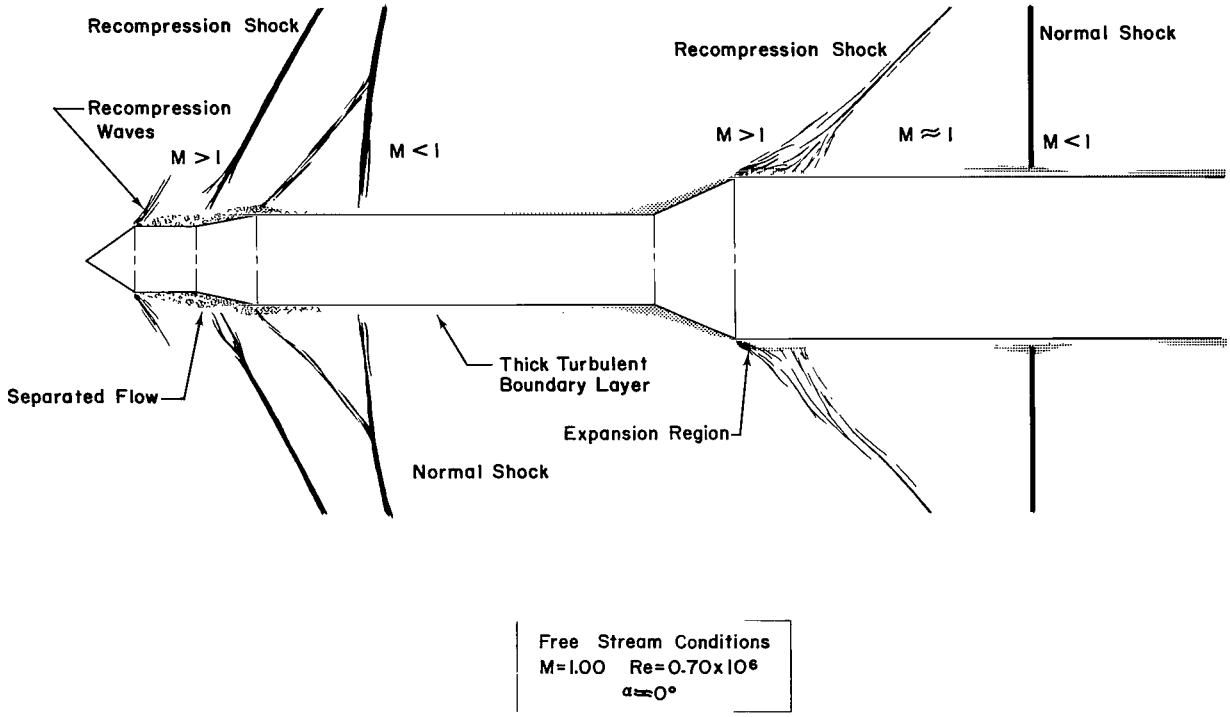

FIGURE 2b. EFFECT OF MACH NUMBER ON UPPER STAGE FLOW FIELDS, CONFIGURATION "A," $\alpha = 0°$

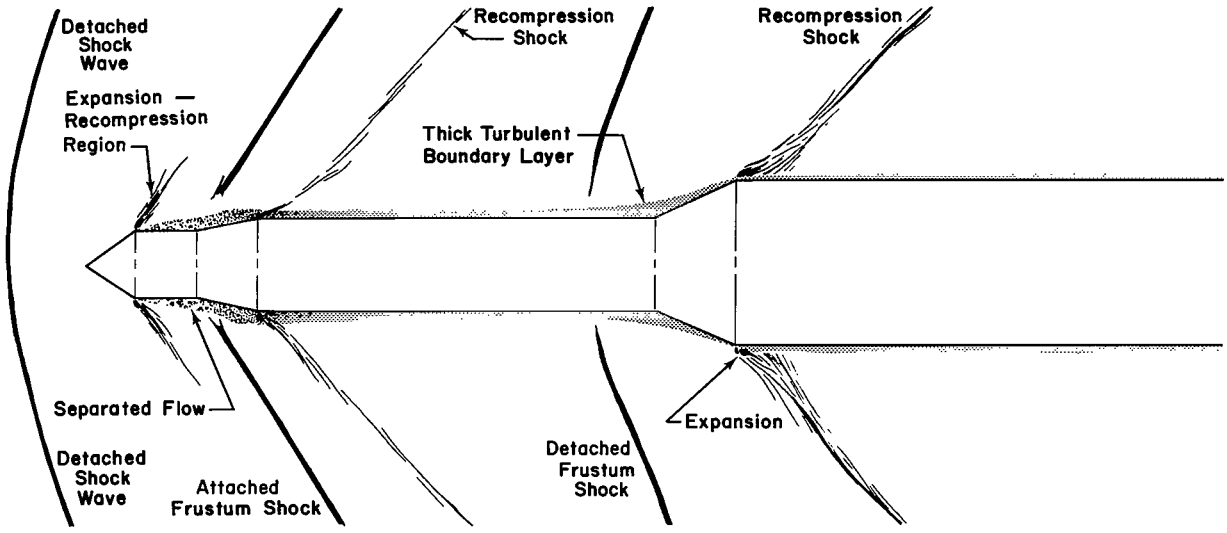

Free Stream Conditions
M=1.10 Re=0.72x10⁶
α≃0°

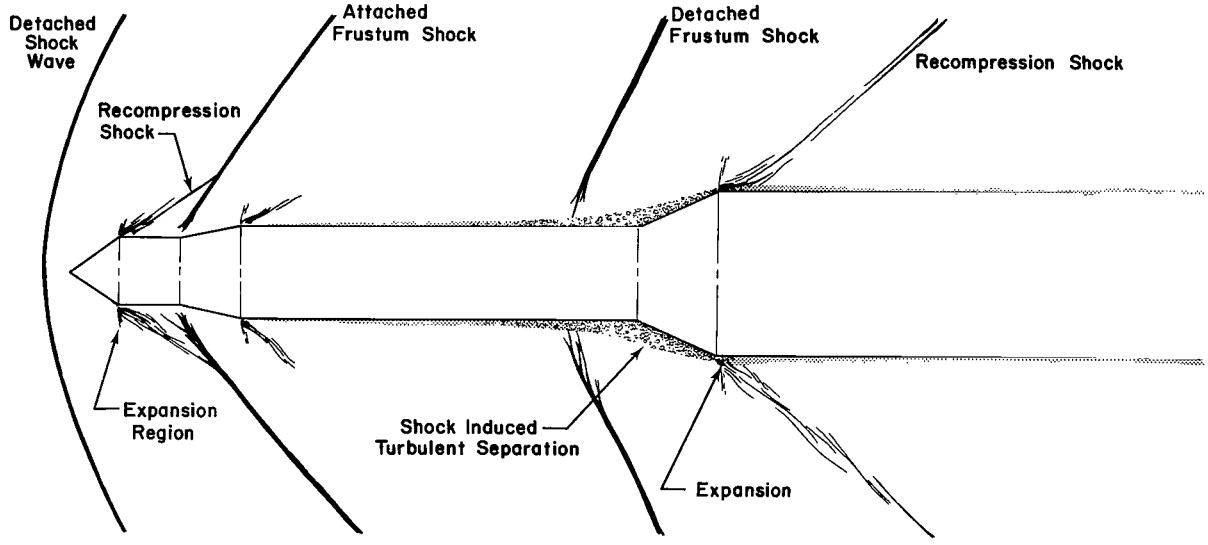

Free Stream Conditions
M=1.20 Re=0.73x10⁶
α≃0°

FIGURE 2c. EFFECT OF MACH NUMBER ON UPPER STAGE FLOW FIELDS, CONFIGURATION "A," $\alpha = 0°$

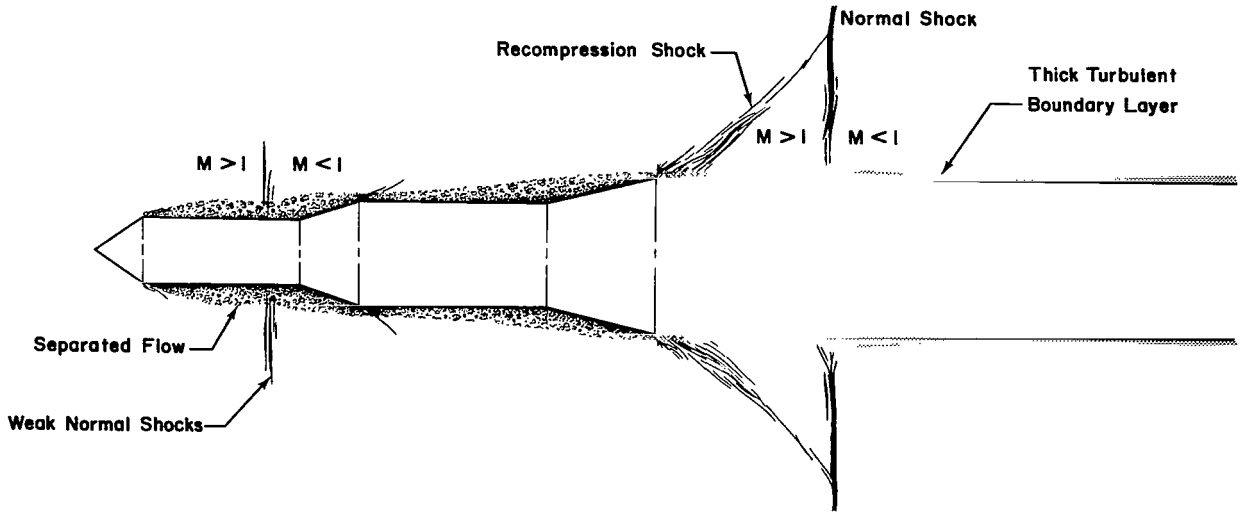

Free Stream Conditions
M = 0.90 Re = 0.68 x 10⁶
α = 0°

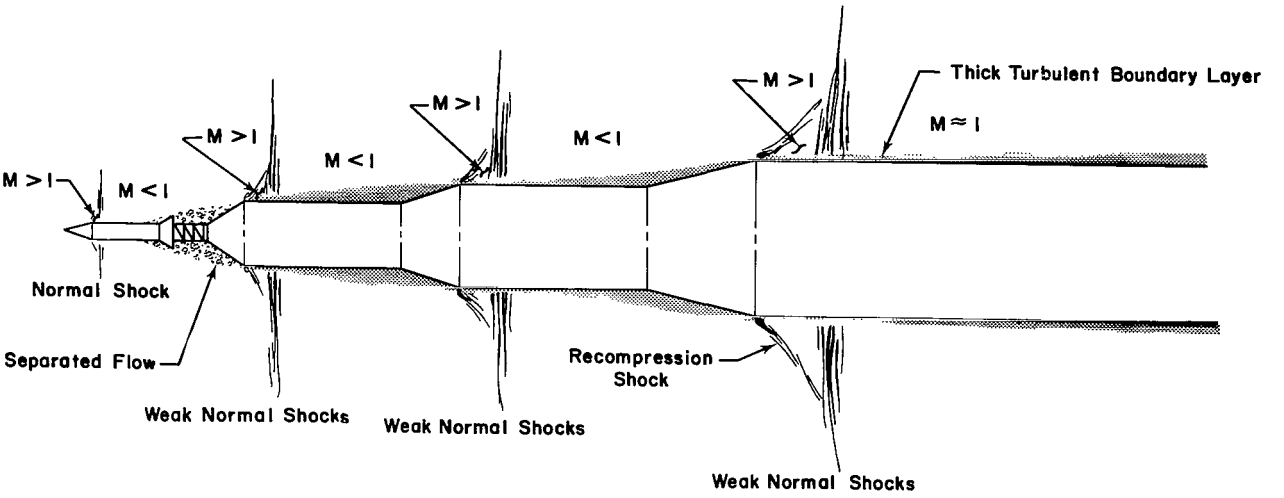

Free Stream Conditions
M = 0.90 Re = 0.68 x 10⁶
α = 0°

FIGURE 3a. EFFECTS OF MACH NUMBER, LAUNCH ESCAPE SYSTEM AND ANGLE OF ATTACK ON UPPER STAGE FLOW FIELDS, CONFIGURATION "B"

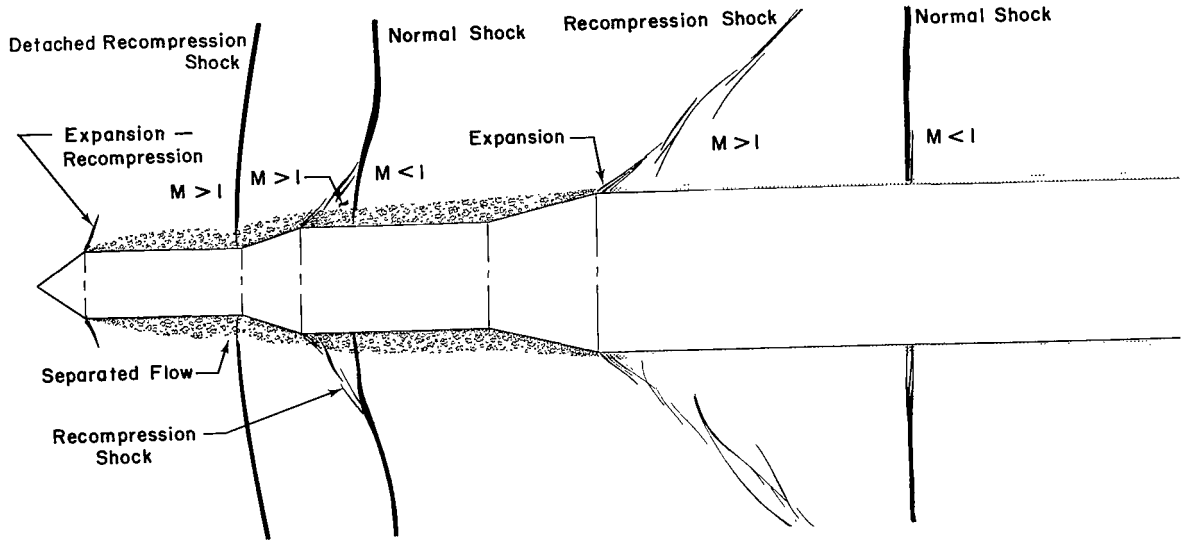

Free Stream Conditions
M = 1.00 Re = 0.70 x 10^6
$\alpha = 0°$

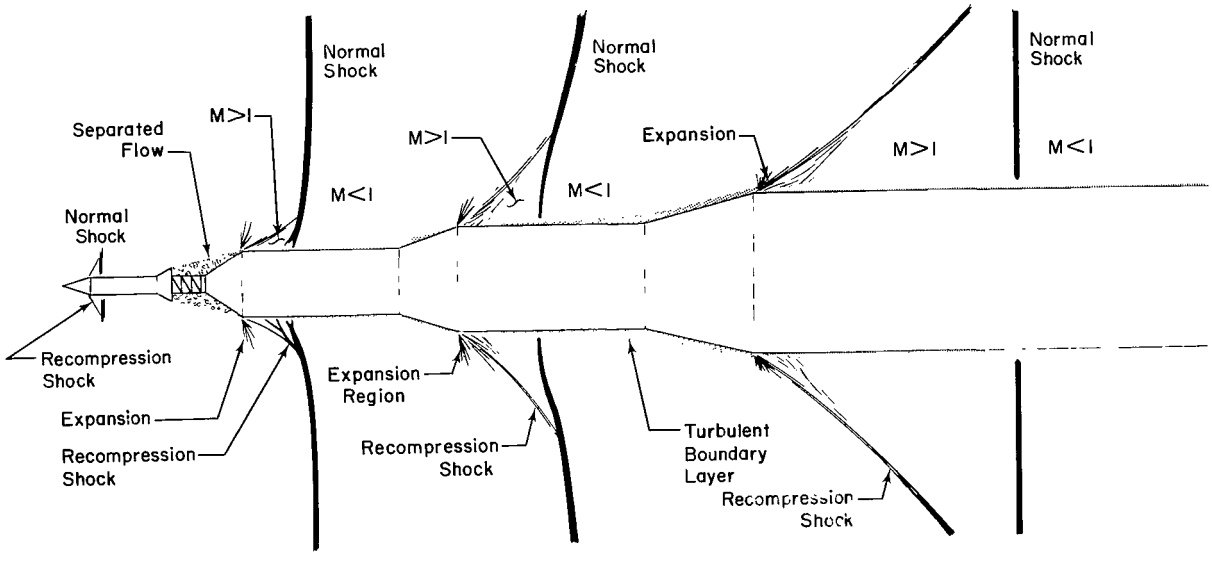

Free Stream Conditions
M = 1.00 Re = 0.70 x 10^6
$\alpha = 0°$

FIGURE 3b. EFFECTS OF MACH NUMBER, LAUNCH ESCAPE SYSTEM AND ANGLE OF ATTACK ON UPPER STAGE FLOW FIELDS, CONFIGURATION "B"

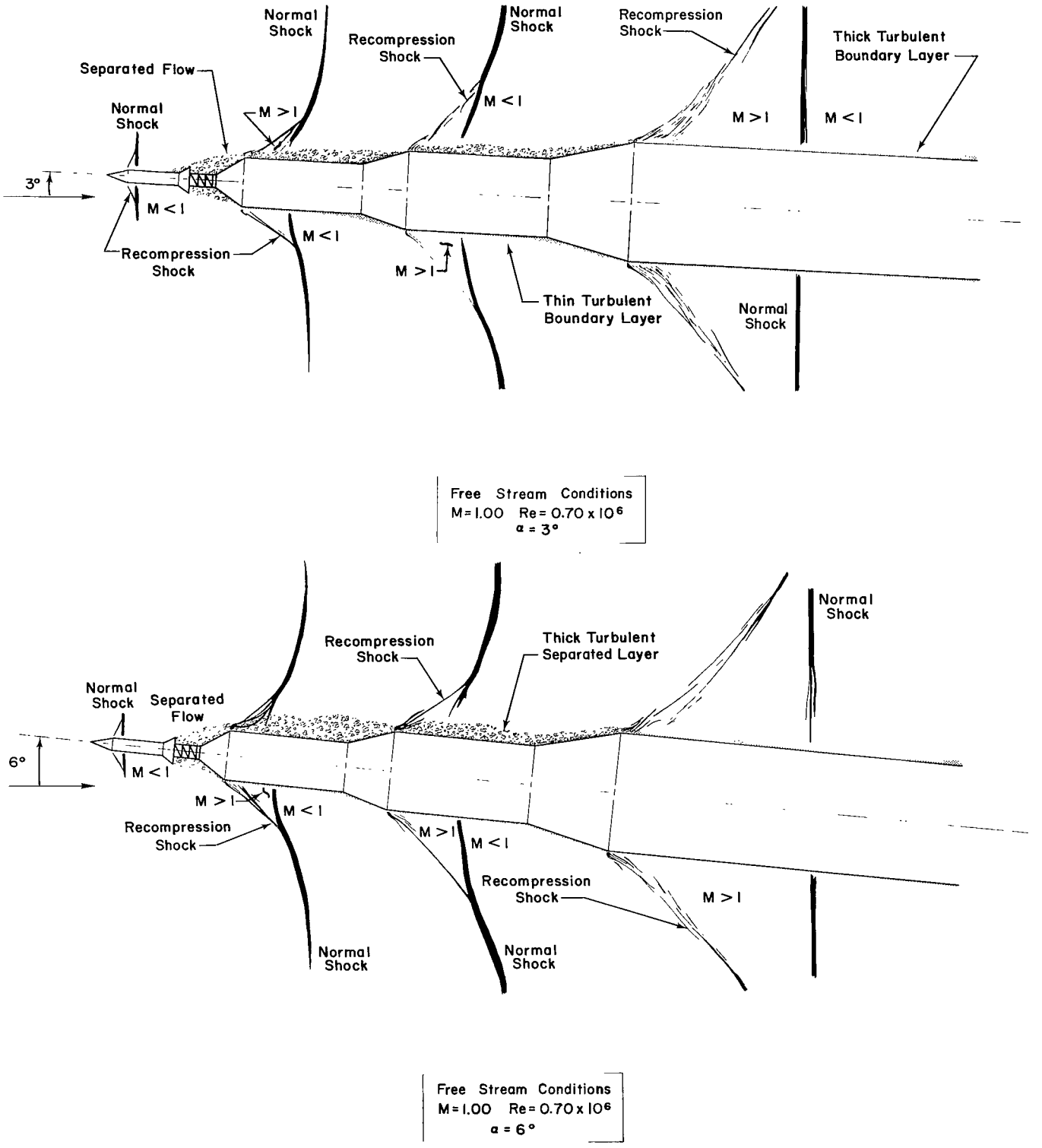

FIGURE 3c. EFFECTS OF MACH NUMBER, LAUNCH ESCAPE SYSTEM AND ANGLE OF ATTACK ON UPPER STAGE FLOW FIELDS, CONFIGURATION "B"

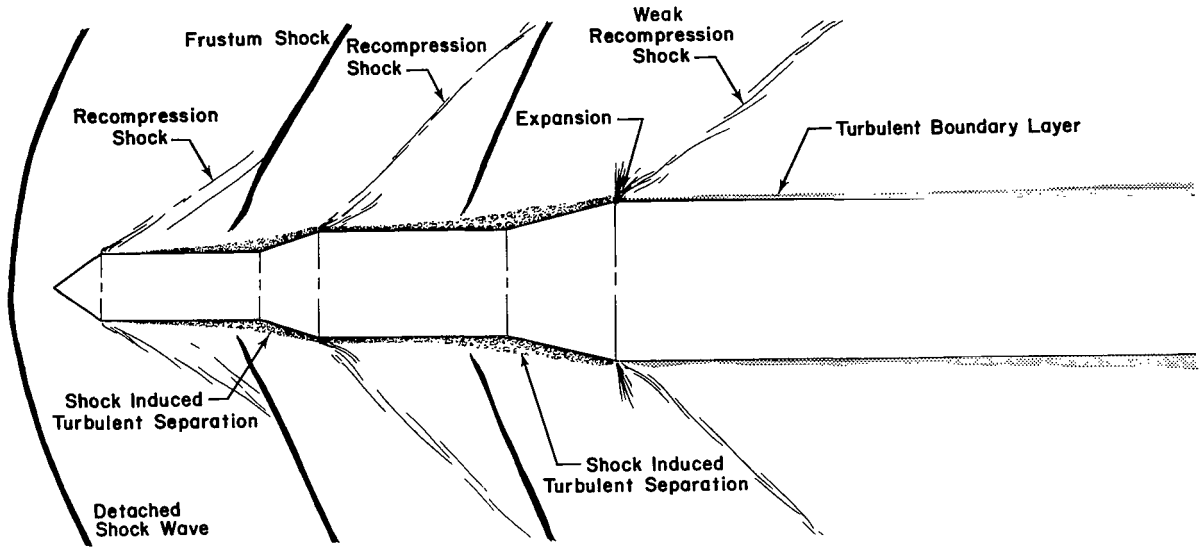

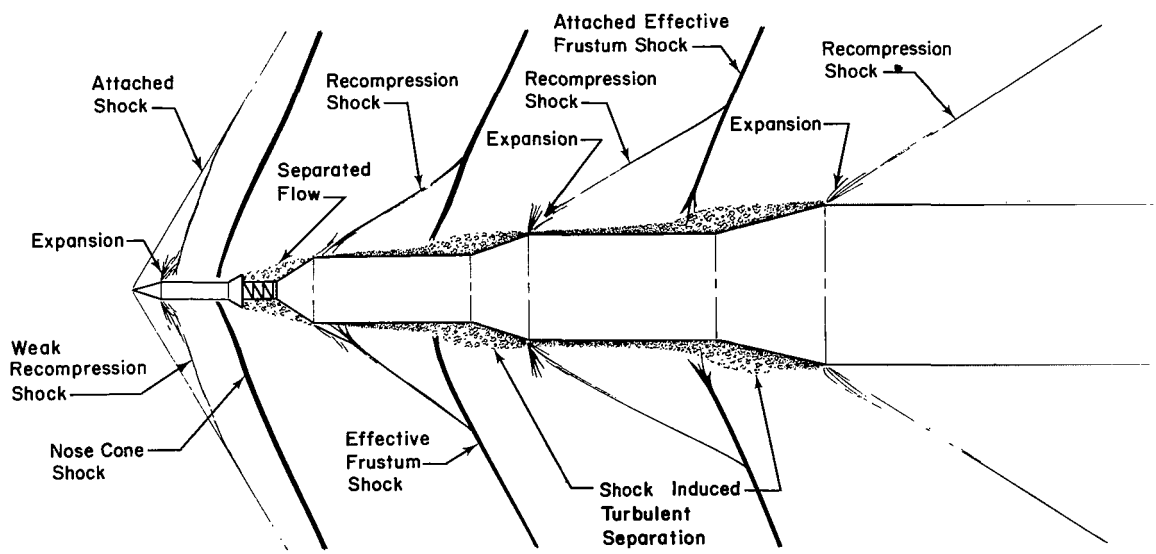

FIGURE 3d. EFFECTS OF MACH NUMBER, LAUNCH ESCAPE SYSTEM AND ANGLE OF ATTACK ON UPPER STAGE FLOW FIELDS, CONFIGURATION "B"

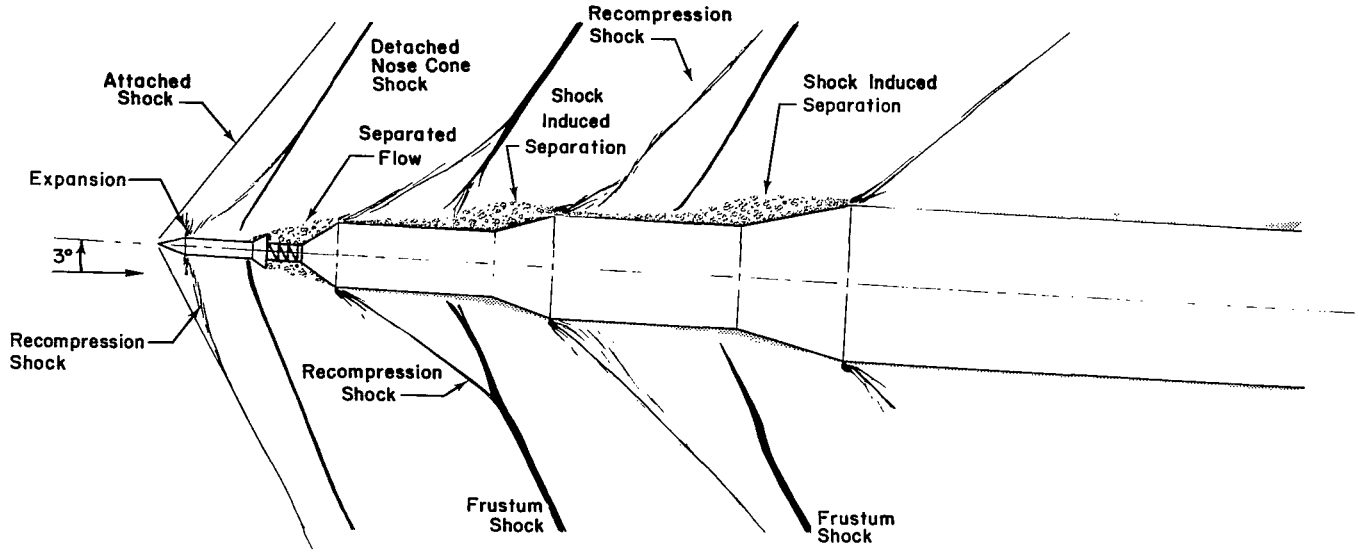

Free Stream Conditions
M = 1.20 Re = 0.72 x 10⁶
α = 3°

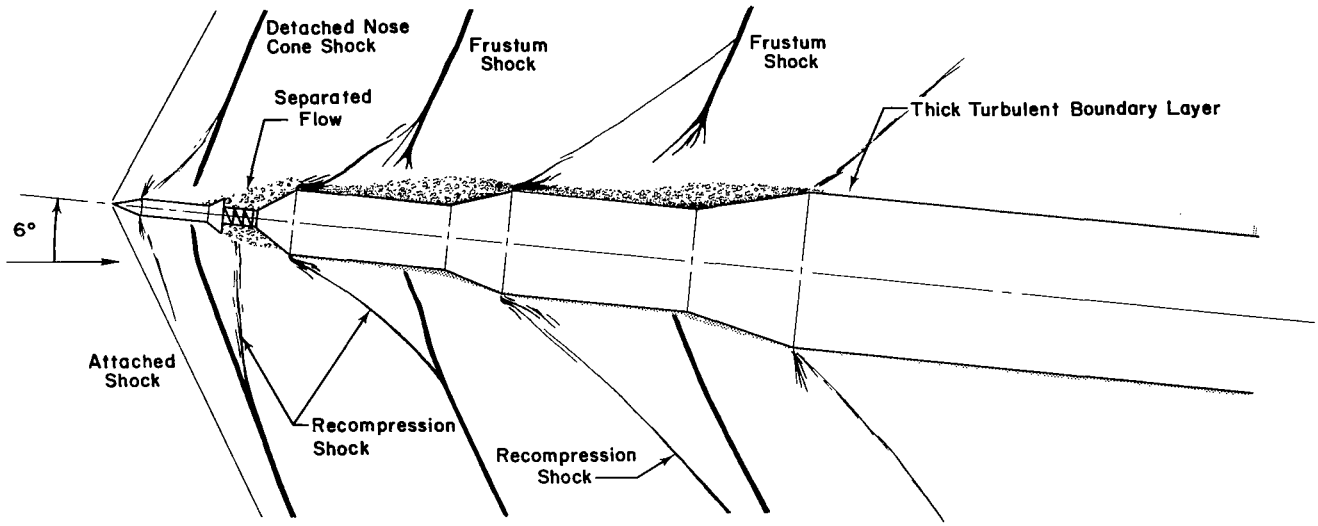

Free Stream Conditions
M = 1.20 Re = 0.72 x 10⁶
α = 6°

FIGURE 3e. EFFECTS OF MACH NUMBER, LAUNCH ESCAPE SYSTEM AND ANGLE OF ATTACK ON UPPER STAGE FLOW FIELDS, CONFIGURATION "B"

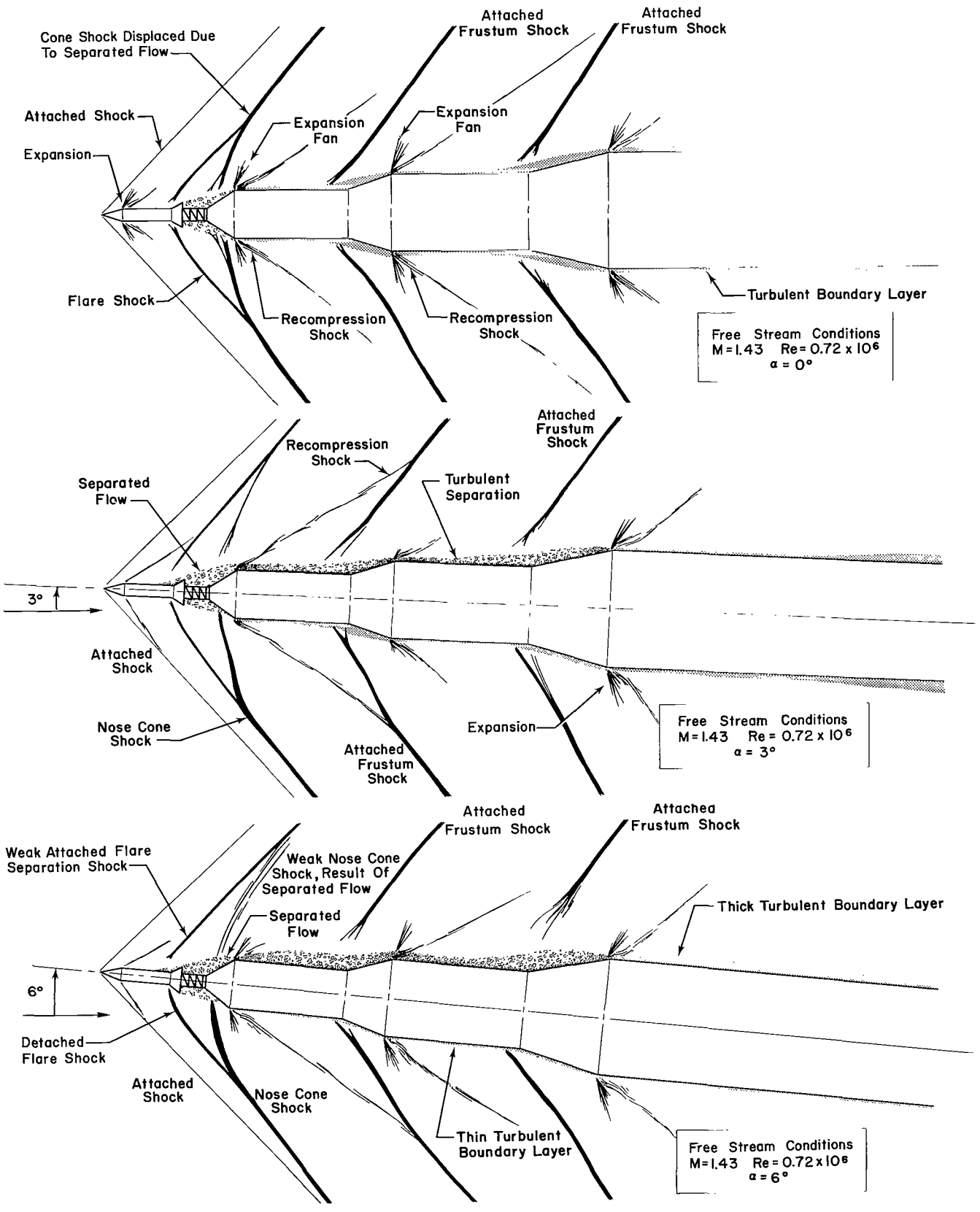

FIGURE 3f. EFFECTS OF MACH NUMBER, LAUNCH ESCAPE SYSTEM AND ANGLE OF ATTACK ON UPPER STAGE FLOW FIELDS, CONFIGURATION "B"

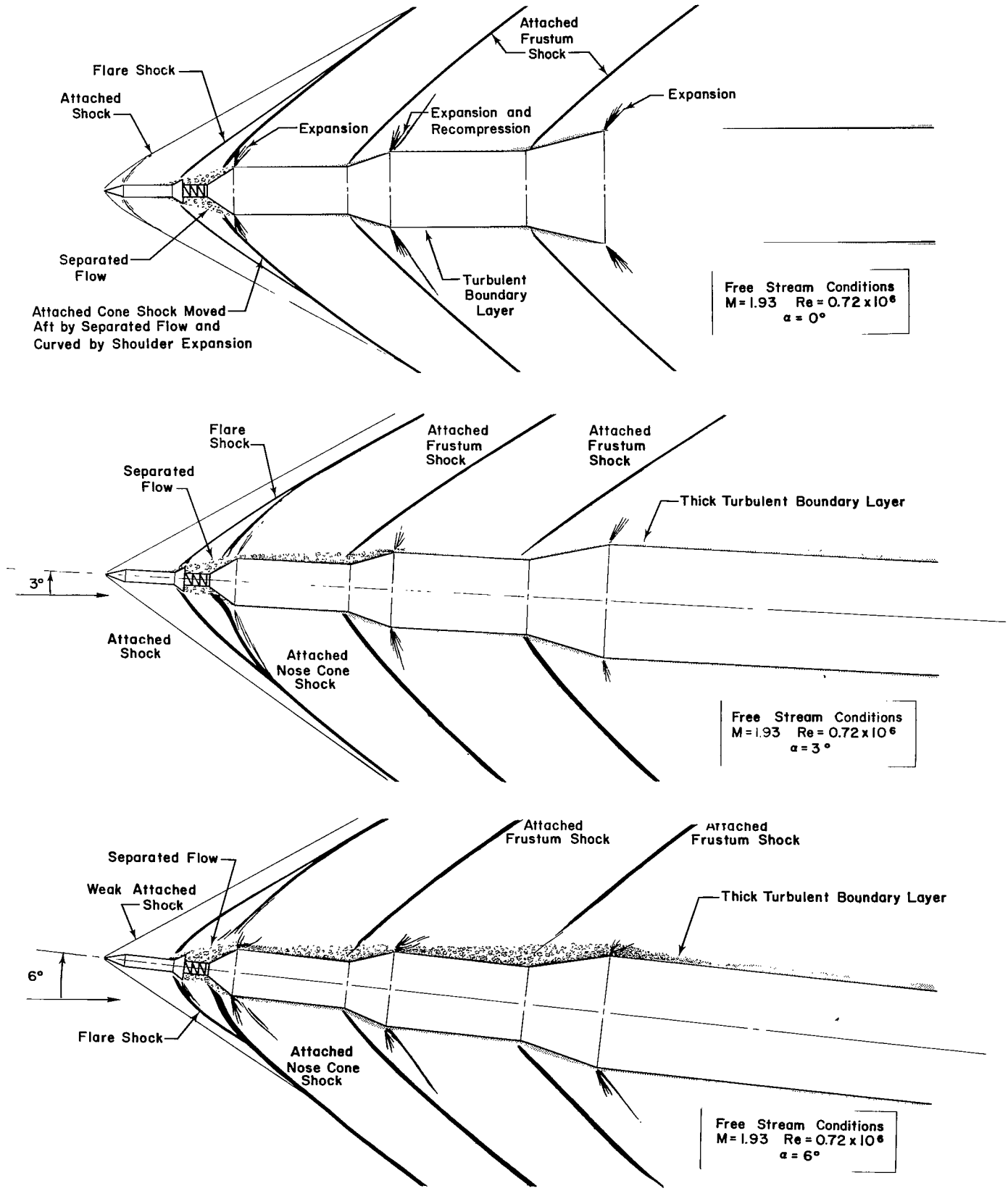

FIGURE 3g. EFFECTS OF MACH NUMBER, LAUNCH ESCAPE SYSTEM AND ANGLE OF ATTACK ON UPPER STAGE FLOW FIELDS, CONFIGURATION "B"

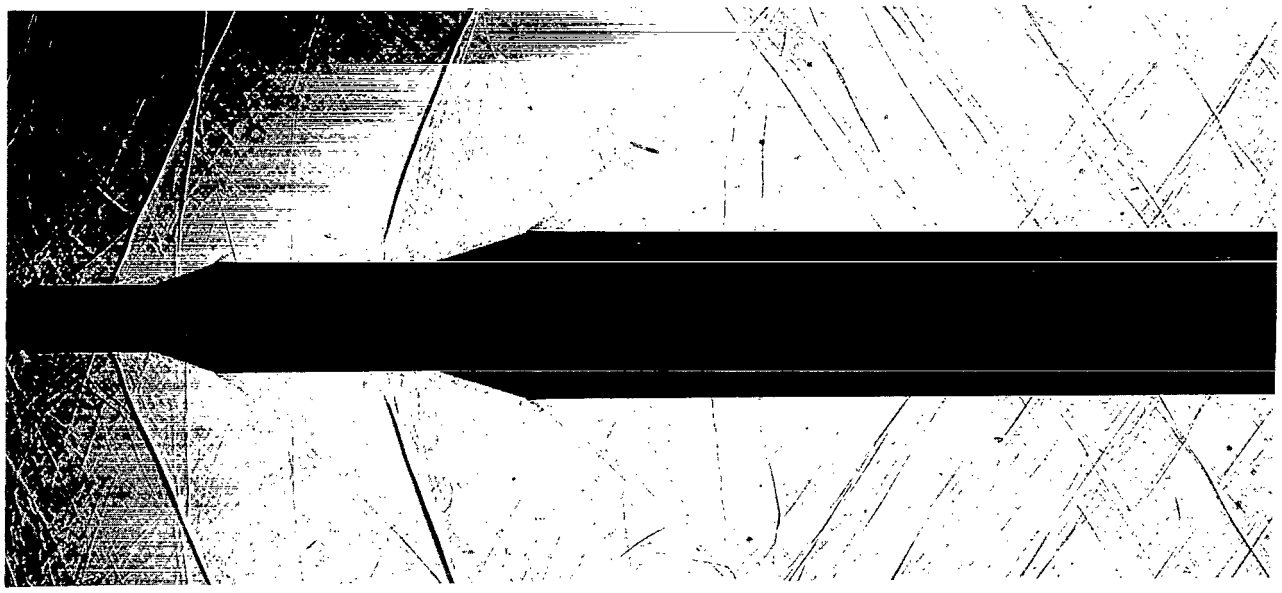

Configuration "B" (w/o LES)

M = 1.20 R_e = 0.72 X 10^6 $\alpha \approx 0°$

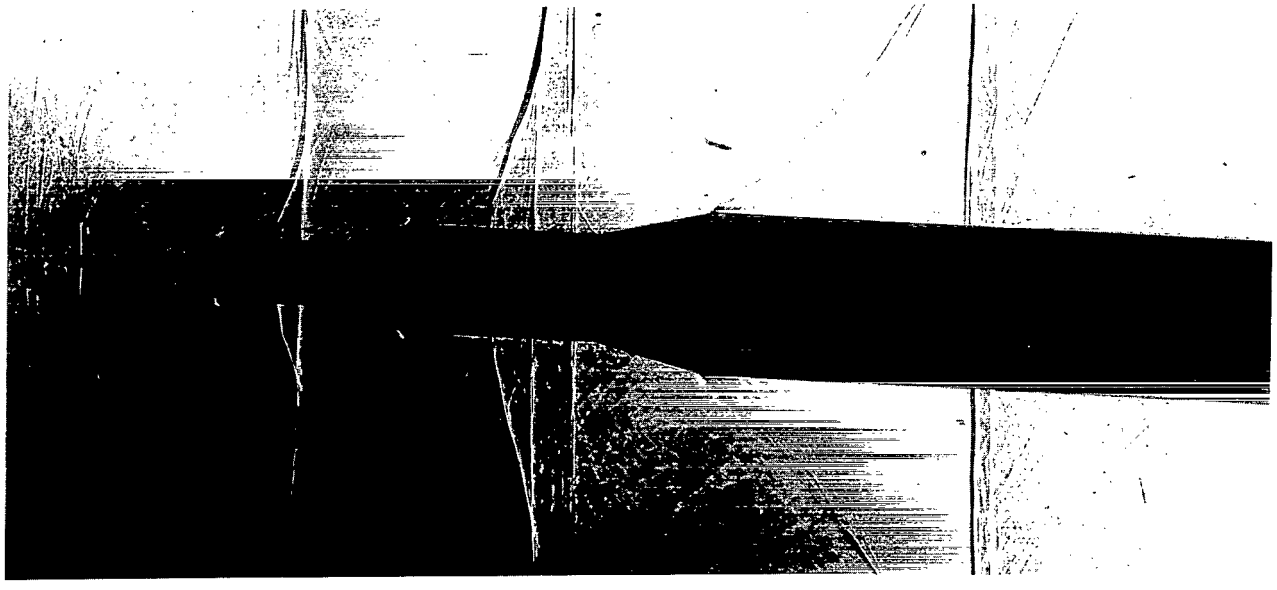

Configuration "B" (w/ LES)

M = 1.00 R_e = 0.70 X 10^6 $\alpha \approx 3°$

FIGURE 4. TYPICAL SHADOWGRAPHS USED TO DETERMINE THE CONSTRUCTION OF THE ENGINEERING INTERPRETATIONS

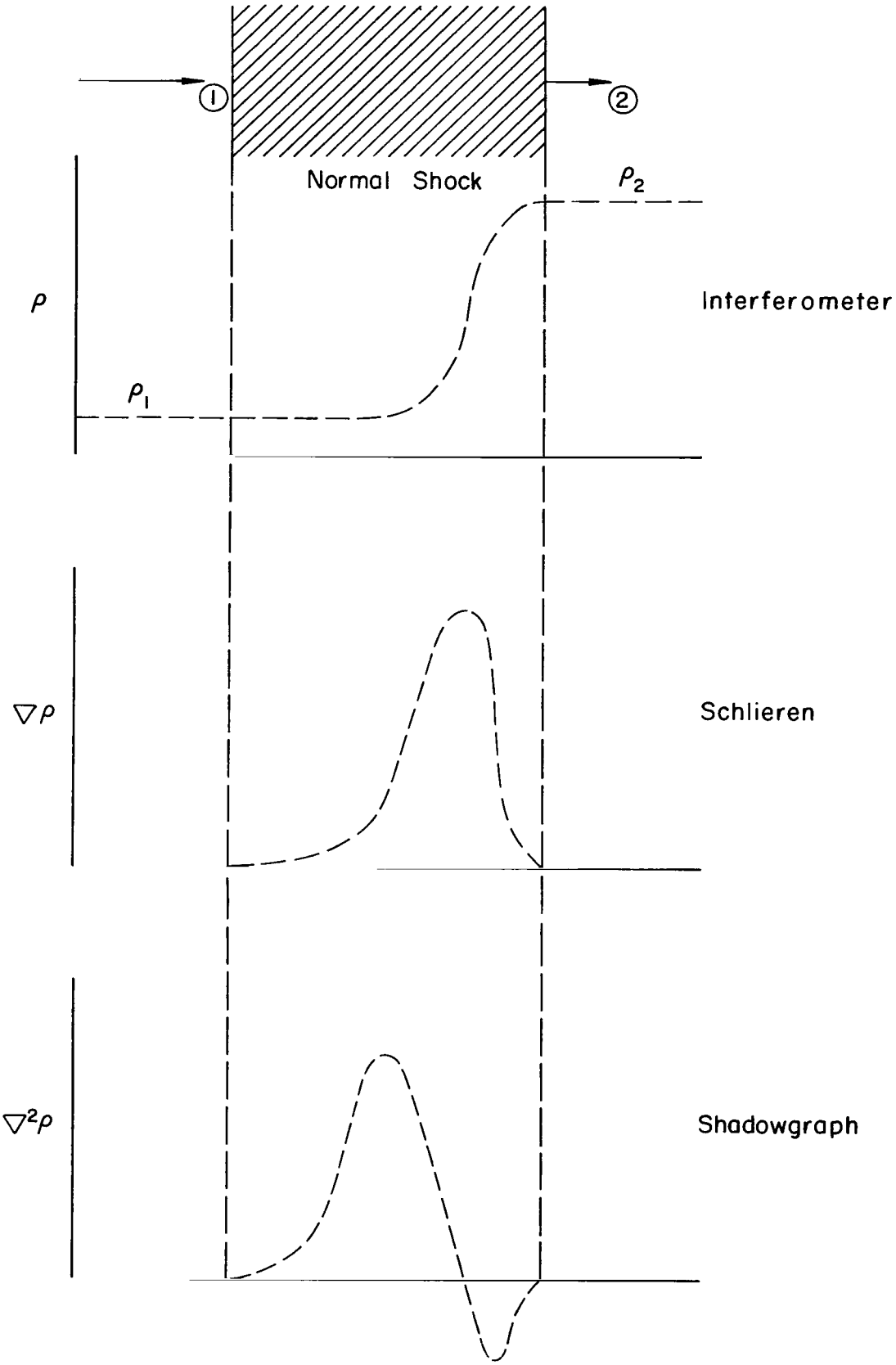

FIGURE 5. TYPICAL NORMAL-SHOCK DENSITY PROFILES AND APPLICABLE FLOW-VISUALIZATION TECHNIQUES

REFERENCES

1. Clark, J. W., J. P. Heaman, and D. L. Stewart, "14-Inch Wind Tunnel Spark Shadowgraph System," NASA TM X-53195, January 22, 1965, Unclassified.

2. May, Ellery B. and William D. Murphree, "Results of Flow Calibrations in the ABMA 14 x 14-Inch Trisonic Wind Tunnel," ABMA-DA-TN-65-58, September 15, 1958, Unclassified.

3. Schlichting, Hermann, Boundary Layer Theory, 4th Edition, Translated by J. Kestin, New York: McGraw-Hill Book Company, Inc., 1960, Unclassified.

4. Carlson, David R., "Results of a Static Longitudinal Stability and Drag Investigation of the Saturn IB Second Stage Performed in the MSFC 14-Inch Trisonic Tunnel at Mach Numbers Between 1.93 and 4.96," M-AERO-E-252-63, September 30, 1963, Unclassified.

5. Kuehn, Donald M., "Turbulent Boundary Layer Separation Induced by Flares on Cylinders at Zero Angle of Attack," NASA TR R-117, 1961, Unclassified.

2/22/25

"The aeronautical and space activities of the United States shall be conducted so as to contribute . . . to the expansion of human knowledge of phenomena in the atmosphere and space. The Administration shall provide for the widest practicable and appropriate dissemination of information concerning its activities and the results thereof."

—NATIONAL AERONAUTICS AND SPACE ACT OF 1958

NASA SCIENTIFIC AND TECHNICAL PUBLICATIONS

TECHNICAL REPORTS: Scientific and technical information considered important, complete, and a lasting contribution to existing knowledge.

TECHNICAL NOTES: Information less broad in scope but nevertheless of importance as a contribution to existing knowledge.

TECHNICAL MEMORANDUMS: Information receiving limited distribution because of preliminary data, security classification, or other reasons.

CONTRACTOR REPORTS: Technical information generated in connection with a NASA contract or grant and released under NASA auspices.

TECHNICAL TRANSLATIONS: Information published in a foreign language considered to merit NASA distribution in English.

TECHNICAL REPRINTS: Information derived from NASA activities and initially published in the form of journal articles.

SPECIAL PUBLICATIONS: Information derived from or of value to NASA activities but not necessarily reporting the results of individual NASA-programmed scientific efforts. Publications include conference proceedings, monographs, data compilations, handbooks, sourcebooks, and special bibliographies.

Details on the availability of these publications may be obtained from:

SCIENTIFIC AND TECHNICAL INFORMATION DIVISION

NATIONAL AERONAUTICS AND SPACE ADMINISTRATION

Washington, D.C. 20546